

Comparative quantitative analysis of optical coherence tomography angiography in varied morphologies of macular neovascularization following intravitreal conbercept and ranibizumab treatments for neovascular age-related macular degeneration

JING LI^{1,2}, ZHUFANG YANG^{1,2}, XUEYING LI¹, DI LI¹, JIN YANG¹ and MEIJIA DANG²

¹Department of Ophthalmology, Shaanxi Provincial People's Hospital, Xi'an, Shaanxi 710068;

²Xi'an Medical College, Xi'an, Shaanxi 710021, P.R. China

Received October 7, 2023; Accepted February 23, 2024

DOI: 10.3892/etm.2024.12501

Abstract. The present study aimed to examine the optical coherence tomography angiography (OCTA) parameters associated with macular neovascularization (MNV) in patients diagnosed with neovascular age-related macular degeneration (nAMD) and treated with either intravitreal conbercept (IVC) or ranibizumab (IVR). It enrolled 39 nAMD patients presenting with MNV, including 23 in the IVC group and 16 in the IVR group. All participants were treatment-naïve with intravitreal therapy and they underwent treatment following a '3+PRN' regimen. The MNV patterns identified through OCTA were categorized as Medusa, tangled, seafan and other variations. Key outcome measures encompassed best-corrected visual acuity (BCVA), MNV vascular area (MNV-VA), MNV vascular density (MNV-VD) ratio and central macular thickness (CMT). In the present study, 44 eyes were included, with 28 eyes undergoing treatment with IVC and 18 eyes with IVR. On day 90, there was a statistically significant improvement in mean BCVA from baseline among all patients treated with IVC ($P=0.002$). Notably, improved outcomes were observed in those with the 'tangled' pattern compared with the other three patterns ($P=0.007$). CMT exhibited a significant decrease from baseline ($P=0.007$), with consistent improvement observed across all four patterns ($P=0.052$) on day 90. The mean MNV-VA decreased in all patients, reaching statistical significance for the Medusa pattern ($P=0.008$), although the improvement in visual acuity was deemed unsatisfactory.

Patients with the seafan pattern treated with IVR improved significantly in BCVA ($P=0.042$). The mean CMT significantly improved from baseline ($P=0.001$), consistent across the four patterns ($P=0.114$). Significant improvements were noted in the mean MNV-VA for the seafan pattern and in the mean MNV-VD ratio for the other patterns. The two regimens had no significant differences regarding BCVA, CMT, and MNV parameters. Conbercept emerged as a viable treatment option for patients presenting with tangled MNV patterns. On the other hand, ranibizumab might be considered an effective intervention for individuals with seafan MNV patterns. Notably, the Medusa MNV pattern was associated with a morphologic configuration indicative of a poor prognosis.

Introduction

Neovascular age-related macular degeneration (nAMD), also known as exudative AMD, is a progressive retinal disease characterized by the development of choroidal and/or subretinal neovascularization. This condition is frequently accompanied by serous and hemorrhagic complications, including bleeding in the subretinal or retinal pigment epithelium (RPE) region, as well as the presence of lipid exudation and the accumulation of subretinal fluid. The abnormal structural characteristics of neovascularization trigger a cascade of pathological processes such as exudation, bleeding, organization, and fibrotic scarring, ultimately culminating in the loss of central vision (1,2).

Anti-vascular endothelial growth factor (anti-VEGF) treatment has emerged as the primary and most effective therapeutic approach for nAMD in the clinical setting. This strategy is grounded in the recognition that VEGF plays a crucial role in ocular neovascularization (3-5). First-line intravitreal-injectable anti-VEGF drugs employed for the treatment of nAMD include ranibizumab (manufactured by Genentech, Inc. and Novartis International AG). Ranibizumab is a humanized recombinant monoclonal antibody fragment designed to inhibit human vascular endothelial growth factor A. Additionally, aflibercept (manufactured by Regeneron Pharmaceuticals Inc. and Bayer Healthcare Company Ltd.)

Correspondence to: Professor Jing Li, Department of Ophthalmology, Shaanxi Provincial People's Hospital, 256 Youyi West Road, Xi'an, Shaanxi 710068, P.R. China
E-mail: lix-www@163.com

Key words: macular neovascularization, neovascular age-related macular degeneration, morphological, anti-vascular endothelial growth factor, optical coherence tomography angiography

and conbercept (KH902; marketed as Lumitin and developed by Chengdu Kanghong Biotech, Ltd.) are both soluble fusion protein agents (6).

While anti-VEGF drugs are generally effective in inhibiting the leakage and bleeding associated with macular neovascularization (MNV) in most nAMD patients, responses to anti-VEGF therapy can vary among individuals with MNV. This heterogeneity implies that the pathological basis for this condition is multifactorial in nature. The diagnosis of MNV is typically established using fluorescein angiography (FA) or indocyanine green angiography (ICGA), which dynamically display abnormal vessels and observe vascular leakage. Optical coherence tomography angiography (OCTA), renowned for its high sensitivity in detecting MNV in nAMD, serves as a rapid, safe, non-invasive, and repeatable imaging modality capable of providing detailed visualizations of different MNV types (7,8). Additionally, OCTA allows for the detection and quantification of quantitative information regarding MNV flow and area (9).

Studies have elucidated the morphological features of MNV in nAMD and classified them into types such as 'tangled' or 'glomerulus' and 'seafan' or 'Medusa' using OCTA (10,11). Researchers have examined the evolution of OCTA qualitative and quantitative biomarkers, encompassing branching capillaries, anastomoses and loops, peripheral arcade and hypointense halo for MNV, following anti-VEGF therapy (12,13). However, the variations in OCTA quantitative data for different morphological patterns of MNV following anti-VEGF treatment and their clinical implications remain to be elucidated.

Moreover, the structural and mechanistic differences between conbercept and ranibizumab have not been thoroughly explored in terms of OCTA quantitative outcomes for various morphological patterns of MNV in nAMD. No study to date has reported on the OCTA quantitative outcomes of different morphological patterns of MNV for nAMD treated with intravitreal conbercept (IVC) compared with intravitreal ranibizumab (IVR). Additionally, the relationship between these OCTA quantitative parameters and visual prognosis after different anti-VEGF drug treatments is still under evaluation and remains inconclusive.

The primary objective of the present study was to analyze the outcomes of quantitative parameters identified through OCTA examination following a '3+PRN' regimen of IVC or IVR in patients exhibiting various morphological patterns of MNV. Additionally, the present study aimed to compare the visual prognosis associated with different MNV morphologies following IVC or IVR treatment. Notably, this investigation represented the first attempt, to the best of the authors' knowledge, to assess changes in quantitative parameters among distinct MNV patterns identified by OCTA in nAMD patients treated with conbercept.

Materials and methods

Study design. This prospective, interventional case series study was carried out at Shaanxi Provincial People's Hospital in Xi'an, China. The study received approval from the ethics committee of Shaanxi Provincial People's Hospital [Xi'an, China; approval no. 2022 no. (R002)], and it was conducted

in accordance with the principles outlined in the Declaration of Helsinki. Prior to the intravitreal injection of anti-VEGF agents, written informed consent was obtained from each study subject. It was crucial to emphasize that we had access to information allowing the identification of individual participants both during and after the data collection process.

Study subjects. The present study enrolled 39 patients diagnosed with nAMD who underwent IVR or IVC at Shaanxi Provincial People's Hospital between April 2022 and August 2023. Only treatment-naïve patients, those who had not previously received any treatment for nAMD, were included in the present study. The inclusion criteria for patients with nAMD were as follows: i) Age ≥ 50 years; ii) OCT/OCTA revealing intra/subretinal fluid (IRF/SRF) or retinal pigment epithelium detachment (PED); iii) MNV identified by FA, ICGA, and OCTA [diagnosed and classified by the same retina specialist (Jing Li)]; and iv) the patient clearly displaying either the 'Medusa,' 'seafan,' or 'tangled' type of MNV. Exclusion criteria for this study included: i) Systemic and ocular diseases causing changes in fundus vasculopathy (e.g., diabetic retinopathy, retinal vascular obstruction); ii) another ocular maculopathy causing MNV [e.g., polypoidal choroidal vasculopathy (PCV), myopic maculopathy, central serous chorioretinopathy, and macular telangiectasia]; iii) hazy media causing refractive stroma and inability to cooperate with the examination; and iv) a history of previous eye surgery or therapy except for cataract (e.g., vitrectomy, photodynamic therapy, other drug injection).

Treatment. A total of 26 eyes of 23 patients received treatment with conbercept (0.5 mg/0.05 ml), while 18 eyes of 16 patients were treated with ranibizumab (0.5 mg/0.05 ml). The intravitreal injection procedure was consistently performed by the same retina specialist (Jing Li). The treatment protocols adhered to the '3+PRN' regimen. All intravitreal injections were conducted as strict aseptic operations following topical administration using povidone-iodine. A topical antibiotic, levofloxacin, was administered 3 days before or after the injection. Comprehensive preoperative and postoperative ophthalmologic examinations were conducted for all patients, including slit-lamp biomicroscopy and dilated fundus examination.

Data collection, image acquisition and analysis. The baseline characteristics of all enrolled patients, encompassing age, sex and past medical history, were meticulously recorded. Best-corrected visual acuity (BCVA) was measured and documented by the same clinician, with subsequent conversion according to the minimum resolution angle logarithm (logMAR) visual acuity.

Central macular thickness (CMT), defined as the distance between the internal limiting membrane (ILM) and the RPE, was measured using a 512x128 scanning mode. The depth enhancement technique, combined with the artifact removal model, was employed to track the retina within the deep macular 6x6 mm² region until two scans of satisfactory quality were obtained (14). The OCT-based optical microangiography (OMAG) algorithm facilitated the detection of amplitude and phase changes between continuous B-scans at the same

position, enabling quantification of motion contrast and generating the OCTA image (15).

The OCTA images were analyzed using the built-in OCTA software. The RPE layer was manually divided to extract the optimal profile image, and the boundary line was fine-tuned manually to exhibit the clearest MNV morphology. A total of six images at the same RPE level were acquired to minimize errors. The images were saved in a standardized format and then imported into ImageJ (v1.54a) software (National Institutes of Health) for thresholding and binarization of pixel intensity.

Each image was magnified 800 times, and the MNV blood vessel area was measured by manually sketching the visible blood vessels with a line of 1 pixel wide. The vascular density ratio was defined as the ratio of the total pixel area within the scanned 6x6 mm² area occupied by vessels in red pixels. The scale conversion relationship was established as 68.8335 (pixel)=1 mm.

All patients, including those diagnosed with nAMD and MNV, underwent comprehensive examinations conducted by the same retina specialist (Jing Li), using OCTA and OCT imaging (CIRRUS HD-OCT model 5000 with AngioPlex[®]; Carl Zeiss Meditec AG). Baseline and structural data were collected before the injection (T1) and at 1 (T2), 7 (T3), 30 (T4), 60 (T5) and 90 days (T6) post anti-VEGF treatment and subsequently analyzed. Comparisons were made between pre-treatment and post-treatment measurements for BCVA, MNV vascular area (MNV-VA), MNV vascular density (MNV-VD) ratio, and CMT.

Morphological patterns of the MNV complex on OCTA were systematically examined and categorized into four groups: i) The 'Medusa' pattern, characterized by branching vessels radiating in all directions from the main vessel trunk at the center; ii) the 'seafan' pattern, defined as a lesion with branching vessels radiating from one side of the main vessel trunk; iii) the 'tangled' pattern, described as a lesion with globular structures of entwined vessels without a discernible main vessel trunk (16); and iv) the 'other' pattern, encompassing lesions with irregular vessels that cannot be attributed to the aforementioned three forms but remain measurable.

Statistical analysis. All statistical analyses were performed using SPSS 26.0 (IBM Corp.). Non-parametric statistical methods were employed, including the Wilcoxon signed-rank test for comparing within-group differences in different morphology groups before and after treatment, Fisher's exact test for categorical variables, and Friedman's test for continuous variables.

To evaluate differences among the four OCTA pattern groups after baseline correction, the present study employed backward elimination of generalized estimating equation (GEE) modeling. Confidence intervals (CIs) were computed using GEE modeling, incorporating the elapsed time since enrollment, treatment assignment and the interaction between time and treatment in the model. In all models, the variable of disease severity was introduced into the constructed GEE model and, after model evaluation, this non-significant contributing factor (impact) was removed by gradually eliminating it. Meanwhile, the present study adjusted for age, sex, BMI, hypertension, diabetes, coronary heart disease and smoking

exposure. Potential confounders were selected a priori. Models were fully adjusted for all covariates simultaneously. $P < 0.05$ was considered to indicate a statistically significant difference.

Results

The baseline characteristics of the study participants are summarized in Table I. No significant differences in age or sex were observed between the IVC treatment group and the IVR treatment group. The analysis included 39 nAMD patients, comprising 17 men and 22 women, with a total of 44 eyes of interest exhibiting MNV. Stratification revealed 26 eyes from 23 patients in the IVC group and 18 eyes from 16 patients in the IVR group.

In the IVC group, the median age of patients was 61 years (range, 50-83), with 13 males and 10 females. The mean BCVA, CMT, MNV-VA, and MNV-VD ratio values were 0.97 ± 0.50 logMAR, 293.71 ± 145.60 μm , 1.34 ± 1.14 mm² and 0.40 ± 0.10 , respectively. Among the 26 eyes displaying a distinct MNV complex on OCTA, the Medusa, seafan, tangled, and other patterns were identified in nine eyes (34.6%), nine eyes (34.6%), five eyes (19.2%) and three eyes (11.5%), respectively.

The IVR group consisted of four men and 12 women, with a mean age of 71.61 ± 11.05 years (range 51-91). Baseline BCVA, CMT, MNV-VA, and MNV-VD ratio values in this group were 0.94 ± 0.54 logMAR, 328.72 ± 144.80 μm , 0.87 ± 0.71 mm², and 0.39 ± 0.06 , respectively. Among the 18 eyes with MNV in this group, the Medusa, seafan, tangled, and other patterns were observed in three eyes (16.7%), seven eyes (38.9%), five eyes (27.8%) and three eyes (16.7%), respectively. All enrolled patients were monitored for 3 months, and no ocular or systemic adverse events were recorded.

Comparisons of outcomes in the IVC treatment group. A total of 26 eyes of 23 patients underwent primary IVC treatment. At the 90-day follow-up, the mean BCVA in the overall cohort improved from 0.97 ± 0.50 logMAR at baseline to 0.78 ± 0.53 logMAR at the last visit ($P = 0.004$). Significant reductions were observed in the mean CMT (from 293.71 ± 145.60 μm to 211.94 ± 51.11 μm ; $P = 0.007$), the mean MNV-VA (from 1.34 ± 1.14 mm² to 0.79 ± 0.59 mm²; $P = 0.001$), and the mean MNV-VD ratio (from 0.40 ± 0.10 to 0.34 ± 0.12 ; $P = 0.037$) post-treatment compared with baseline.

Specifically, the mean BCVA of eyes with the tangled pattern improved from 0.86 ± 0.60 logMAR at baseline to 0.41 ± 0.38 logMAR at the last visit ($P = 0.002$). Notably, the improvement in BCVA was significantly higher in patients with the tangled pattern compared with the other three patterns. The change associated with the tangled pattern was -0.43 ± 0.13 (95% CI, -0.7 to -0.17 ; $P = 0.001$) compared with the Medusa pattern group, -0.30 ± 0.13 (95% CI, -0.57 to -0.04 ; $P = 0.023$) compared with the seafan pattern group, and -0.34 ± 0.13 (95% CI, -0.61 to -0.08 ; $P = 0.01$) compared with the other pattern group.

While the mean CMTs of the four MNV patterns decreased following treatment, there was no significant difference in the total change of CMT between the different pattern groups ($P = 0.052$). Regarding MNV parameters, eyes with the Medusa pattern showed a significant reduction in mean MNV-VA at the last visit (from 2.18 ± 1.36 mm² to 0.92 ± 0.74 mm²; $P = 0.008$).

Table I. Baseline characteristics of neovascular age-related macular degeneration patients receiving intravitreal conbercept or ranibizumab.

Characteristic	Intravitreal conbercept	Intravitreal ranibizumab	P-value
No. of eyes (patients)	26 (23)	18 (16)	-
Age, years	71.15±10.04	71.61±11.05	0.895
Sex (male:female)	13:10	4:12	0.099
BMI, kg/m ²	23.62±3.23	23.87±3.60	0.784
HBP	13 (50%)	11 (61.1%)	0.547
DM	7 (26.9%)	2 (11.1%)	0.270
IRF	9 (34.6%)	9 (50%)	0.361
SRF	11 (42.3%)	8 (44.4%)	1.000
Mean BCVA (LogMA)	0.97±0.50	0.94±0.54	0.831
Mean CMT, μ m	293.71±145.60	328.72±144.80	0.527
Mean MNV-VA, mm ²	1.34±1.14	0.87±0.71	0.166
Mean MNV-VD ratio	0.40±0.10	0.39±0.06	0.596

Baseline data are presented as means \pm standard deviation for both groups. $P < 0.05$ was considered to indicate a statistically significant difference. BMI, body mass index; HBP, high blood pressure; DM, diabetes mellitus; IRF, intraretinal fluid; SRF, subretinal fluid; BCVA, best-corrected visual acuity; CMT, central macular thickness; MNV, macular neovascularization; MNV-VA, MNV vascular area; MNV-VD ratio, MNV vascular density ratio.

The change degree analysis indicated that the reduction in the Medusa pattern group was -1.04 ± 0.40 mm² (95% CI, -1.82 to -0.27 ; $P = 0.008$) compared with the tangled pattern group, -1.03 ± 0.50 mm² (95% CI, -2 to -0.05 ; $P = 0.038$) compared with the seafan pattern group, and -1.25 ± 0.41 mm² (95% CI, -2.05 to -0.45 ; $P = 0.002$) compared with the other pattern group. Consequently, patients with the Medusa pattern in the IVC group experienced the most substantial reduction in mean MNV-VA.

The mean MNV-VD ratios for all four MNV patterns showed a decrease at the last visit after treatment compared with baseline, with the most notable reduction observed in the Medusa pattern group. However, these changes in all MNV patterns did not reach statistical significance ($P = 0.107$). Figs. 1 and 2, and Tables II-V illustrate the comparisons of BCVA, CMT, and MNV parameters between pre- and post-IVC treatment at various time points in the four MNV pattern groups on OCTA. Tables II and IV describe the mean, while Tables III and V reflect the difference in change compared with baseline. Additionally, Fig. 3 presents an illustrative case of a patient with a tangled pattern MNV.

Comparisons of outcomes in the IVR treatment group. A total of 18 eyes of 16 patients underwent primary IVR treatment. At the 90-day follow-up, the mean BCVA in the overall cohort improved from 0.94 ± 0.54 logMAR at baseline to 0.70 ± 0.47 logMAR at the last visit ($P = 0.014$). Notable reductions were observed in the mean CMT (from 328.72 ± 144.80 μ m to 200.51 ± 90.29 μ m; $P = 0.001$), the mean MNV-VA (from 0.87 ± 0.71 mm² to 0.47 ± 0.35 mm²; $P = 0.133$), and the mean MNV-VD ratio (from 0.39 ± 0.06 to 0.31 ± 0.11 ; $P = 0.05$).

The improvements in mean BCVA and CMT between pre- and post-treatment were statistically significant in the overall cohort, whereas changes in mean MNV-VA and MNV-VD ratio were not. The mean BCVA of eyes with the seafan pattern

improved from 0.94 ± 0.40 logMAR at baseline to 0.50 ± 0.32 logMAR at the last visit ($P = 0.042$). The improvement in BCVA was significantly greater for the seafan pattern compared with the other three patterns. Specifically, the change in the seafan pattern group was -0.48 ± 0.10 (95% CI, -0.69 to -0.28 ; $P = 0.00$) compared with the Medusa pattern group, -0.13 ± 0.18 (95% CI, -0.48 to 0.22 ; $P = 0.469$) compared with the tangled pattern group, and -0.44 ± 0.20 (95% CI, -0.61 to -0.08 ; $P = 0.01$) compared with the other pattern group.

The mean CMT in all four MNV pattern groups exhibited a decrease post-treatment, with the most prominent reduction observed in the other pattern group. However, there was no statistically significant difference in the total change in CMT among the various pattern groups ($P = 0.114$). Regarding MNV parameters, the mean MNV-VA for all four pattern groups decreased after treatment, with the most substantial reduction observed in the seafan pattern group (from 1.33 ± 0.90 mm² to 0.57 ± 0.41 mm²; $P = 0.225$). The degree of reduction in the seafan pattern group was -0.73 ± 0.44 mm² (95% CI, -1.6 to 0.13 ; $P = 0.095$) compared with the Medusa pattern group, -0.16 ± 0.45 mm² (95% CI, -1.05 to 0.73 ; $P = 0.722$) compared with the tangled pattern group, and -1.04 ± 0.41 mm² (95% CI, -1.85 to -0.23 ; $P = 0.012$) compared with the other pattern group.

The mean MNV-VD ratios for all four pattern groups exhibited a decrease at the last visit after treatment, with the most significant reduction observed in the other pattern group (from 0.40 ± 0.01 to 0.28 ± 0.04 ; $P = 0.109$). However, there was no statistically significant difference in the total change in the MNV-VD ratio among the different pattern groups. Figs. 4 and 5, and Tables VI-IX depict the comparisons of BCVA, CMT, and MNV parameters between pre- and post-treatment at various time points in the four MNV pattern groups on OCTA. Additionally, Fig. 6 illustrates a representative case of a patient with a seafan pattern MNV.

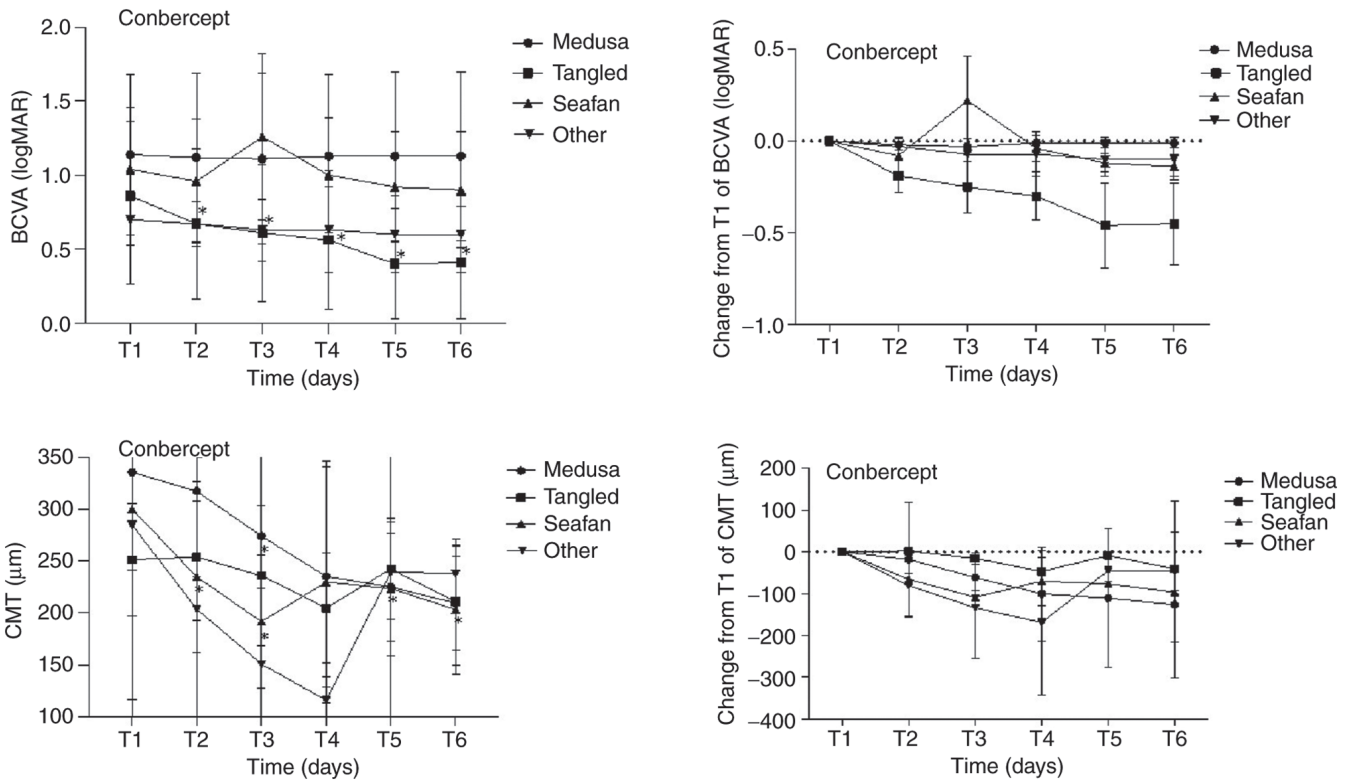


Figure 1. Comparison of BCVA and CMT before and after treatment for eyes with four distinct MNV patterns observed on OCTA. The top row presents mean BCVA values (left) and adjusted mean changes in BCVA (right) from baseline to post-treatment at different time points. The bottom row displays mean CMT values (left) and adjusted mean changes in CMT (right) from baseline to post-treatment at various time points. BCVA, best-corrected visual acuity; CMT, central macular thickness; MNV, macular neovascularization; OCTA, optical coherence tomography angiography.

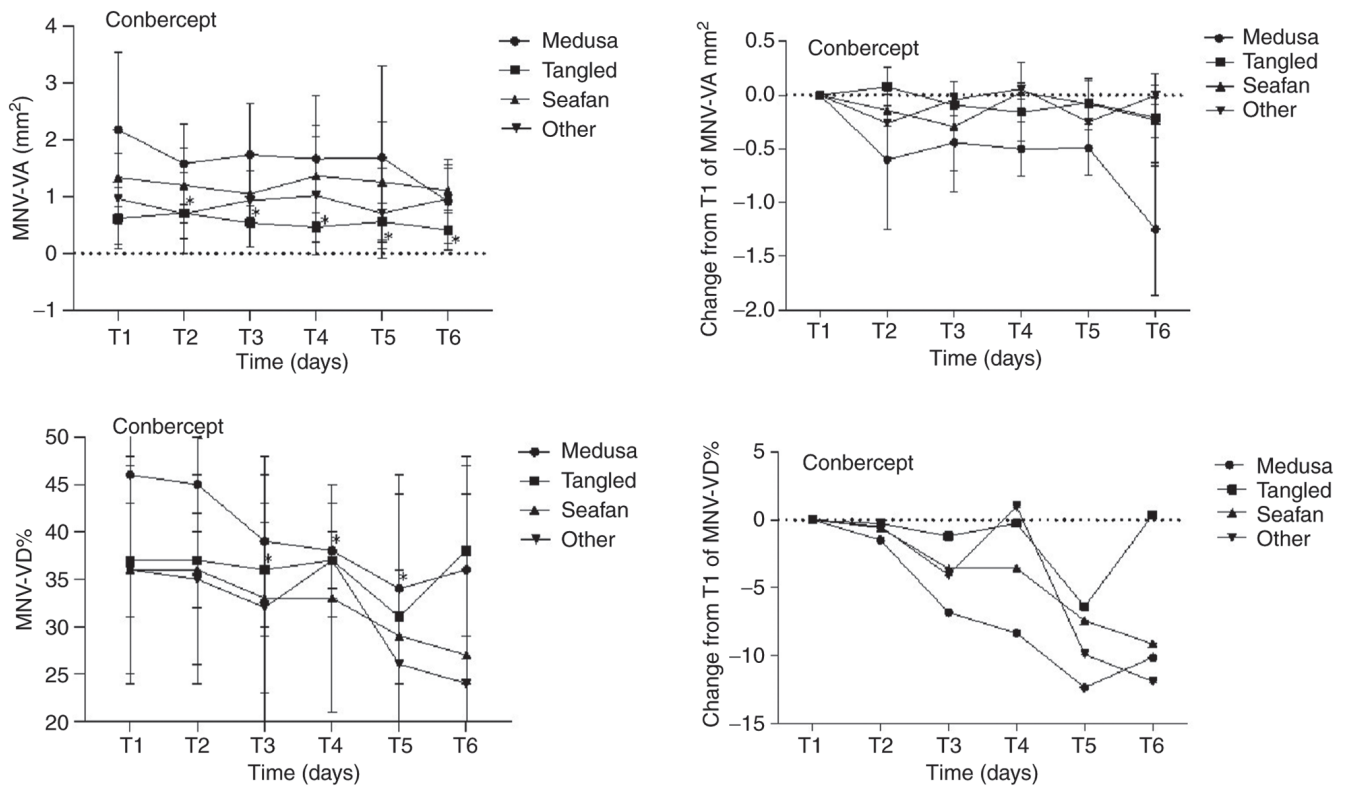


Figure 2. Comparison of MNV parameters before and after treatment for eyes with four distinct MNV patterns of the neovascular membrane, as observed on OCTA. The top row illustrates mean MNV-VA values (left) and adjusted mean changes in mean MNV-VA (right) from baseline to post-treatment at various time points. The bottom row displays mean MNV-VD ratio values (left) and adjusted mean changes in mean MNV-VD ratio (right) from baseline to post-treatment at different time points. MNV, macular neovascularization; OCTA, optical coherence tomography angiography; MNV-VA, MNV vascular area; MNV-VD, MNV vascular density.

Table II. Mean BCVA and CMT of four MNV morphologies at different times after intravitreal conbercept treatment.

Time (post-injection)	Medusa (n=9)			Tangled (n=9)			Seafan (n=5)			Other (n=3)		
	BCVA		P-value	BCVA		P-value	BCVA		P-value	BCVA		P-value
	(logMAR)	CMT (μ m)		(logMAR)	CMT (μ m)		(logMAR)	CMT (μ m)		(logMAR)	CMT (μ m)	
T1 (0 day)	1.14±0.54	335.56±219.14	0.86±0.60	251.28±54.19	1.04±0.32	300.20±58.66	0.70±0.17	284.67±195.09				
T2 (1 day)	1.12±0.57	317.11±182.09	0.499	253.78±61.48	0.859	234.63±72.90	0.043	203.67±123.09				
T3 (7 days)	1.11±0.58	274.11±186.71	0.012	235.67±67.55	0.214	191.58±63.92	0.043	150.67±73.19				
T4 (30 days)	1.13±0.55	235.00±106.13	0.11	204.67±53.12	0.086	229.72±116.20	0.225	115.67±22.50				
T5 (60 days)	1.13±0.57	224.85±52.20	0.214	242.44±48.80	0.374	223.40±64.62	0.043	239.53±155.73				
T6 (90 days)	1.13±0.57	209.42±44.89	0.173	210.72±60.72	0.051	203.20±62.85	0.043	237.77±26.79				

Data are presented as means \pm standard deviation. T1 (day 0) is presented as the baseline. $P < 0.05$ was considered to indicate a statistically significant difference. BCVA, best-corrected visual acuity; CMT, central macular thickness; MNV, macular neovascularization.

Table III. Changes from baseline in mean BCVA and CMT of four MNV morphologies at different times after intravitreal conbercept treatment.

Time (post-injection)	Medusa (n=9)			Tangled (n=9)			Seafan (n=5)			Other (n=3)				
	BCVA		P-value	BCVA		P-value	BCVA		P-value	BCVA		P-value		
	(logMAR)	CMT (μ m)		(logMAR)	CMT (μ m)		(logMAR)	CMT (μ m)		(logMAR)	CMT (μ m)			
T2 (1 day)	-0.02±0.01	-18.44±16.88	0.499	-0.19±0.07	0.026	2.49±9.76	0.859	-0.08±0.05	0.18	-65.57±9.67	0.043	-0.03±0.03	0.317	-81.00±34.29
T3 (7 days)	-0.03±0.02	-61.44±17.66	0.012	-0.24±0.08	0.018	-15.62±10.83	0.214	0.22±0.12	0.102	-108.62±16.41	0.043	-0.07±0.03	0.157	-134.00±59.38
T4 (30 days)	-0.01±0.01	-100.56±52.49	0.11	-0.30±0.09	0.024	-46.62±27.29	0.086	-0.04±0.04	0.317	-70.48±45.88	0.225	-0.07±0.05	0.317	-169.00±81.37
T5 (60 days)	-0.01±0.02	-110.71±73.17	0.214	-0.46±0.13	0.012	-8.84±11.37	0.374	-0.12±0.03	0.063	-76.8±19.11	0.043	-0.10±0.05	0.180	-45.14±27.61
T6 (90 days)	-0.01±0.05	-126.14±72.97	0.173	-0.44±0.13	0.007	-40.56±16.16	0.051	-0.14±0.05	0.066	-97.00±13.60	0.043	-0.10±0.05	0.180	-46.90±87.75

Data are presented as means \pm standard deviation. $P < 0.05$ was considered to indicate a statistically significant difference. BCVA, best-corrected visual acuity; CMT, central macular thickness; MNV, macular neovascularization.

Table IV. Mean MNV-VA and MNV-VD of four MNV morphologies at different times after intravitreal conbercept treatment.

Time (post-injection)	Medusa (n=9)			Tangled (n=9)			Seafan (n=5)			Other (n=3)		
	MNV-VA (mm ²)	MNV-VD ratio	P-value	MNV-VA (mm ²)	MNV-VD ratio	P-value	MNV-VA (mm ²)	MNV-VD ratio	P-value	MNV-VA (mm ²)	MNV-VD ratio	P-value
T1 (0 day)	2.18±1.36	0.46±0.09	0.678	0.62±0.53	0.37±0.06	0.953	1.34±0.82	0.36±0.11	0.5	0.36±0.12	0.36±0.11	0.109
T2 (1 day)	1.58±0.71	0.45±0.05	0.139	0.71±0.71	0.37±0.05	0.161	1.20±0.67	0.36±0.10	0.5	0.35±0.11	0.36±0.10	0.109
T3 (7 days)	1.74±0.90	0.39±0.09	0.021	0.54±0.43	0.36±0.07	0.314	1.05±0.41	0.33±0.13	0.893	0.32±0.09	0.33±0.13	0.18
T4 (30 days)	1.67±1.11	0.38±0.05	0.038	0.46±0.26	0.37±0.06	0.859	1.37±0.88	0.33±0.12	0.5	0.37±0.03	0.33±0.12	0.18
T5 (60 days)	1.69±1.61	0.34±0.10	0.008	0.56±0.33	0.31±0.13	0.066	1.26±1.06	0.29±0.17	0.5	0.26±0.10	0.29±0.17	0.285
T6 (90 days)	0.92±0.74	0.36±0.12	0.139	0.41±0.34	0.38±0.09	0.859	1.11±0.39	0.27±0.17	0.5	0.24±0.05	0.27±0.17	0.593

Data are presented as mean ± standard deviation. P<0.05 was considered to indicate a statistically significant difference. MNV-VA, MNV vascular area; MNV-VD, MNV vascular density; MNV, macular neovascularization.

Table V. Changes from baseline in mean MNV-VA and MNV-VD of four MNV morphologies at different times after intravitreal conbercept treatment.

Time (post-injection)	Medusa (n=9)			Tangled (n=9)			Seafan (n=5)			Other (n=3)		
	MNV-VA (mm ²)	MNV-VD ratio	P-value	MNV-VA (mm ²)	MNV-VD ratio	P-value	MNV-VA (mm ²)	MNV-VD ratio	P-value	MNV-VA (mm ²)	MNV-VD ratio	P-value
T2 (1 day)	-0.60±0.25	-1.49±2.10	0.678	0.08±0.11	-0.28±1.23	0.499	-0.14±0.22	-0.60±1.08	0.5	-0.03±0.03	-0.03±0.03	0.109
T3 (7 days)	-0.44±0.37	-6.81±4.39	0.441	-0.09±0.09	-1.20±0.37	0.161	-0.29±0.29	-3.57±1.17	0.5	-0.07±0.03	-0.07±0.03	0.180
T4 (30 days)	-0.50±0.47	-8.35±3.68	0.26	-0.16±0.13	-0.26±0.21	0.314	0.03±0.50	-3.56±1.22	0.893	-0.07±0.05	-0.07±0.05	0.180
T5 (60 days)	-0.49±0.53	-12.35±4.75	0.26	-0.07±0.12	-6.39±3.33	0.859	-0.08±0.64	-7.43±8.18	0.5	-0.10±0.05	-0.10±0.05	0.285
T6 (90 days)	-1.25±0.38	-10.13±5.88	0.008	-0.21±0.10	0.37±2.17	0.066	-0.23±0.31	-9.12±7.55	0.5	-0.10±0.05	-0.10±0.05	0.593

Data are presented as mean ± standard deviation. P<0.05 was considered to indicate a statistically significant difference. MNV-VA, MNV vascular area; MNV-VD ratio, MNV vascular density ratio; MNV, macular neovascularization.

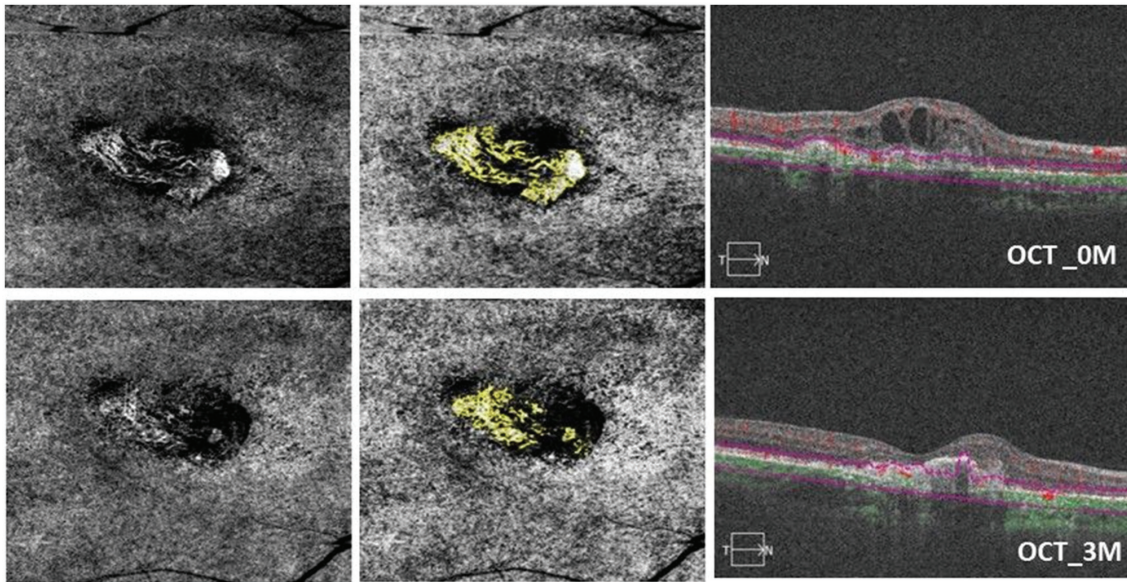


Figure 3. OCTA images of a 52-year-old female patient with a tangled pattern of MNV who underwent IVC therapy in the right eye. Baseline visual acuity was 1.2 logMAR; status, after three conbercept injections in 90 days. In the top left, a 6x6 spectral-domain OCTA image displays the neovascular complex with tangled lesions, showing no main vascular entanglement compared with an OCTA *en face* projection image taken after conbercept injection (bottom left). In the top center, the analysis results of ImageJ software correspond to post-treatment (bottom center). The top right OCT image shows the presence of subretinal fluid. In the bottom right, subretinal fluid was reduced, and BCVA improved to 0.8 logMAR after conbercept injection at 3 months (90 days). The MNV-VA decreased from 1.467 mm² (baseline) to 0.315 mm² (90 days). OCTA, optical coherence tomography angiography; MNV, macular neovascularization; IVC, intravitreal conbercept; MAR, minimum resolution angle; MNV-VA, MNV vascular area.

Comparisons between the two treatment groups. The mean BCVA, CMT, and MNV parameters of the two groups did not exhibit significant differences between pre-injection and the last visit (90 days) after injection. These data are presented in Table X.

Discussion

MNV, formerly known as choroidal neovascularization (CNV), represents a pathological manifestation of nAMD. The updated nomenclature system categorizes MNV into three types: Type 1 MNV encompasses occult CNV and PCV, type 2 MNV corresponds to classic CNV and type 3 MNV primarily involves neovascularization originating from the deep capillary plexus of the retinal circulation and extending towards the outer retina (17). This revision to the standardized nomenclature system reflects the integration of insights derived from recent advancements in imaging technology.

In contemporary fundus disease diagnostics, multimodal imaging technology plays a crucial role. For vascular-related retinal conditions, particularly nAMD, a leading cause of irreversible visual impairment in individuals aged >50 worldwide (18), OCTA has emerged as the primary tool for MNV evaluation and analysis due to its non-invasive and repeatable advantages. Previous studies have highlighted that the detection rate of MNV is influenced by various factors, such as PED, with type 2 MNV being more easily detectable than type 1 MNV. Despite this, the sensitivity of MNV detection by OCTA is comparable to that of ICGA (55-90%), and OCTA excels in identifying the morphology and intricate details of MNV (11,19-22).

The present study enrolled 39 patients with clinically active lesions, achieving an MNV detection rate of 100% using

OCTA. Moreover, a well-defined and clearly distinguishable neovascular complex morphology was identified in 38 out of 44 eyes (86.3%). These findings aligned with the results of previous studies (13,19-22).

Various studies have characterized and assessed MNV based on morphological features detected by OCTA. El Ameen *et al* (23) identified two distinct type 2 morphologies: The Medusa and the glomerulus patterns, typically associated with a main branch. De Carlo *et al* (24) have used a fiber descriptor for MNV morphology. A study conducted by Kuehlewein *et al* (25) found that among highly organized CNV lesions observed through OCTA, 55% exhibit the Medusa type, 21% the seafan type and 24% an indistinct type. However, these studies do not delve into the clinical significance of these diverse patterns.

In a retrospective analysis of 184 eyes, Karacorlu *et al* (26) associated type 1, type 2 and mixed-type neovascularization with nAMD using OCTA. They found that all clinically active cases display well-defined patterns, such as Medusa and seafan patterns. Conversely, 47% of clinically inactive cases exhibit an ill-defined, unidentifiable morphology. The findings of their study suggest that the morphological characteristics observed through OCTA are not inherently linked to clinical activity. However, a notable exception is the association of long, dilated filamentous linear vessels with chronicity and lesion inactivity.

Tew *et al* (16) further differentiated and reported tangled pattern complexes with a main trunk or feeder vessel. In their study of 140 eyes, they identified MNV in 78.6%, with 37.3% displaying the Medusa pattern, 39.1% the seafan pattern and 23.6% the tangled pattern. In the present study, 27.2% of eyes exhibited the Medusa pattern, 36.3% the seafan pattern, 22.7% the tangled pattern and 13.6% another pattern (i.e., ill-defined

Table VI. Mean BCVA and CMT of four MNV morphologies at different times after intravitreal ranibizumab treatment.

Time (post-injection)	Medusa (n=3)			Tangled (n=7)			Seafan (n=5)			Other (n=3)		
	BCVA (logMAR)	P-value	CMT (μ m)	BCVA (logMAR)	P-value	CMT (μ m)	BCVA (logMAR)	P-value	CMT (μ m)	BCVA (logMAR)	P-value	CMT (μ m)
T1 (0 day)	0.63±0.25	0.317	270.33±62.27	1.20±0.64	0.157	354.71±136.05	0.94±0.40	0.063	286.80±192.45	0.63±0.57	0.655	396.33±161.25
T2 (1 day)	0.67±0.21	0.317	258.00±39.23	1.11±0.67	0.157	313.43±139.30	0.74±0.42	0.063	310.4±250.75	0.684	0.70±0.36	306.00±122.53
T3 (7 days)	0.63±0.49	1	228.40±44.83	0.93±0.51	0.026	287.71±138.56	0.60±0.38	0.041	212.8±70.26	0.138	0.77±0.32	229.33±81.05
T4 (30 days)	0.70±0.44	0.655	253.90±37.34	0.99±0.64	0.173	252.43±165.07	0.64±0.38	0.039	179.00±70.78	0.043	0.73±0.31	183.33±83.72
T5 (60 days)	0.64±0.35	0.785	211.77±14.07	0.96±0.68	0.147	247.43±129.26	0.40±0.30	0.043	162.52±54.81	0.043	0.73±0.31	158.33±7.57
T6 (90 days)	0.68±0.24	0.18	206.54±10.12	0.89±0.66	0.09	248.73±125.54	0.50±0.32	0.042	159.28±52.33	0.043	0.63±0.32	150.67±16.01

Data are presented as means ± standard deviation. T1 (day 0) is presented as the baseline. P<0.05 was considered to indicate a statistically significant difference. BCVA, best-corrected visual acuity; CMT, central macular thickness; MNV, macular neovascularization.

Table VII. Changes from baseline in mean BCVA and CMT of four MNV morphologies at different times after intravitreal ranibizumab treatment.

Time (post-injection)	Medusa (n=3)			Tangled (n=7)			Seafan (n=5)			Other (n=3)			
	BCVA (logMAR)	P-value	CMT (μ m)	BCVA (logMAR)	P-value	CMT (μ m)	BCVA (logMAR)	P-value	CMT (μ m)	BCVA (logMAR)	P-value	CMT (μ m)	
T2 (1 day)	0.03±0.03	0.317	-12.33±16.60	-0.09±0.05	0.157	-41.29±6.57	-0.20±0.07	0.063	23.60±24.05	0.684	0.07±0.14	0.655	-90.33±28.78
T3 (7 days)	0.00±0.14	1	-41.94±33.08	-0.27±0.09	0.026	-67.00±18.34	-0.34±0.06	0.041	-74.00±51.83	0.138	0.13±0.12	0.414	-167.00±62.36
T4 (30 days)	0.07±0.10	0.655	-16.44±16.27	-0.21±0.12	0.173	-102.29±36.08	-0.30±0.06	0.039	-107.80±53.73	0.043	0.10±0.12	0.655	-213.00±97.16
T5 (60 days)	0.00±0.05	0.785	-58.57±29.18	-0.24±0.12	0.147	-107.29±32.49	-0.54±0.09	0.043	-124.28±64.82	0.043	0.10±0.12	0.655	-238±77.76
T6 (90 days)	0.04±0.03	0.18	-63.80±24.79	-0.31±0.15	0.09	-105.98±27.50	-0.44±0.10	0.042	-127.53±68.48	0.043	0.00±0.17	1.000	-245.67±75.42

Data are presented as means ± standard deviation. P<0.05 was considered to indicate a statistically significant difference. BCVA, best-corrected visual acuity; CMT, central macular thickness; MNV, macular neovascularization.

Table VIII. Mean MNV-VA and MNV-VD of four MNV morphologies at different times after intravitreal ranibizumab treatment.

Time (post-injection)	Medusa (n=3)			Tangled (n=7)			Seafan (n=5)			Other (n=3)		
	MNV-VA (mm ²)	MNV-VD ratio	P-value	MNV-VA (mm ²)	MNV-VD ratio	P-value	MNV-VA (mm ²)	MNV-VD ratio	P-value	MNV-VA (mm ²)	MNV-VD ratio	P-value
T1 (0 day)	0.61±0.54	0.41±0.04	0.18	0.87±0.67	0.35±0.06	0.091	1.33±0.90	0.41±0.07	0.225	0.36±0.21	0.40±0.01	0.285
T2 (1 day)	1.19±1.09	0.41±0.04	0.18	0.60±0.50	0.35±0.054	0.091	1.01±0.73	0.40±0.07	0.225	0.85±0.41	0.39±0.01	0.285
T3 (7 days)	0.75±0.59	0.40±0.05	0.18	0.54±0.53	0.33±0.04	0.018	0.59±0.37	0.39±0.05	0.08	0.69±0.35	0.35±0.06	0.109
T4 (30 days)	0.54±0.43	0.38±0.05	0.593	0.70±0.87	0.35±0.06	0.398	0.77±0.74	0.36±0.07	0.08	0.90±0.20	0.36±0.03	0.109
T5 (60 days)	0.42±0.24	0.39±0.09	0.593	0.36±0.12	0.33±0.09	0.043	0.57±0.50	0.34±0.11	0.08	0.74±0.52	0.29±0.01	0.109
T6 (90 days)	0.59±0.45	0.30±0.12	0.109	0.28±0.06	0.35±0.10	0.043	0.57±0.41	0.30±0.17	0.225	0.65±0.48	0.28±0.04	0.109

Data are presented as means ± standard deviation. T1 (day 0) is presented as the baseline. P<0.05 was considered to indicate a statistically significant difference. MNV-VA, MNV vascular area; MNV-VD, MNV vascular density ratio; MNV, macular neovascularization.

Table IX. Changes from baseline in mean MNV-VA and MNV-VD of four MNV morphologies at different times after intravitreal ranibizumab treatment.

Time (post-injection)	Medusa (n=3)			Tangled (n=7)			Seafan (n=5)			Other (n=3)		
	MNV-VA (mm ²)	MNV-VD ratio	P-value	MNV-VA (mm ²)	MNV-VD ratio	P-value	MNV-VA (mm ²)	MNV-VD ratio	P-value	MNV-VA (mm ²)	MNV-VD ratio	P-value
T2 (1 day)	0.58±0.44	-0.20±0.14	0.18	-0.26±0.13	-0.65±0.64	0.091	-0.31±0.21	-0.68±1.01	0.225	0.49±0.21	-0.27±0.15	0.285
T3 (7 days)	0.14±0.20	-1.01±0.38	0.109	-0.32±0.11	-2.80±1.92	0.018	-0.74±0.32	-1.80±2.62	0.08	0.32±0.14	-5.04±2.35	0.109
T4 (30 days)	-0.07±0.09	-3.11±0.43	0.593	-0.16±0.18	-0.62±1.60	0.398	-0.55±0.24	-5.20±3.83	0.08	0.54±0.00	-3.59±1.74	0.109
T5 (60 days)	-0.19±0.18	-2.16±2.5	0.593	-0.51±0.21	-2.46±3.99	0.043	-0.76±0.34	-6.41±7.14	0.08	0.38±0.15	-10.38±0.37	0.109
T6 (90 days)	-0.02±0.20	-11.79±4.27	0.109	-0.59±0.23	-0.80±3.82	0.043	-0.75±0.39	-10.44±9.31	0.225	0.29±0.13	-12.02±1.17	0.109

Data are presented as means ± standard deviation. P<0.05 was considered to indicate a statistically significant difference. MNV-VA, MNV vascular area; MNV-VD, MNV vascular density; MNV, macular neovascularization.

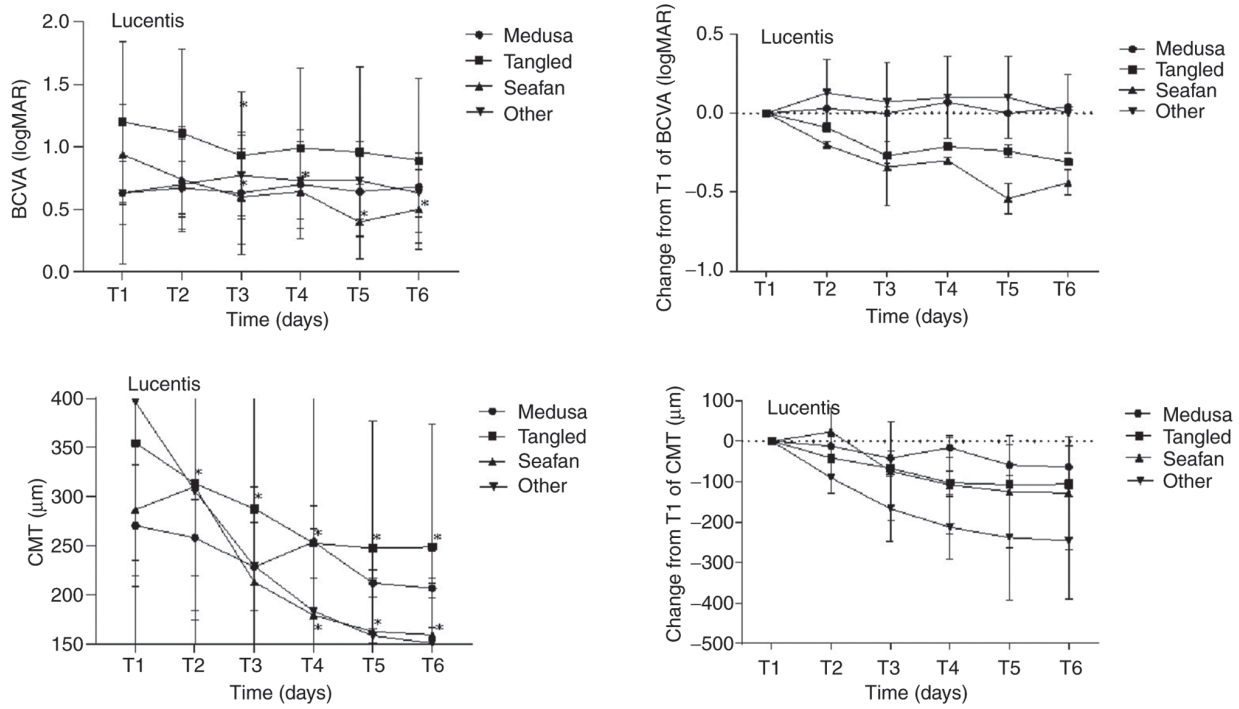


Figure 4. Comparison of BCVA and CMT before and after treatment for eyes with four distinct MNV patterns observed on OCTA. The top row illustrates mean BCVA values (left) and adjusted mean changes in mean BCVA (right) from baseline to post-treatment at various time points. The bottom row displays mean CMT values (left) and adjusted mean changes in mean CMT (right) from baseline to post-treatment at different time points. BCVA, best-corrected visual acuity; CMT, central macular thickness; MAR, minimum resolution angle.

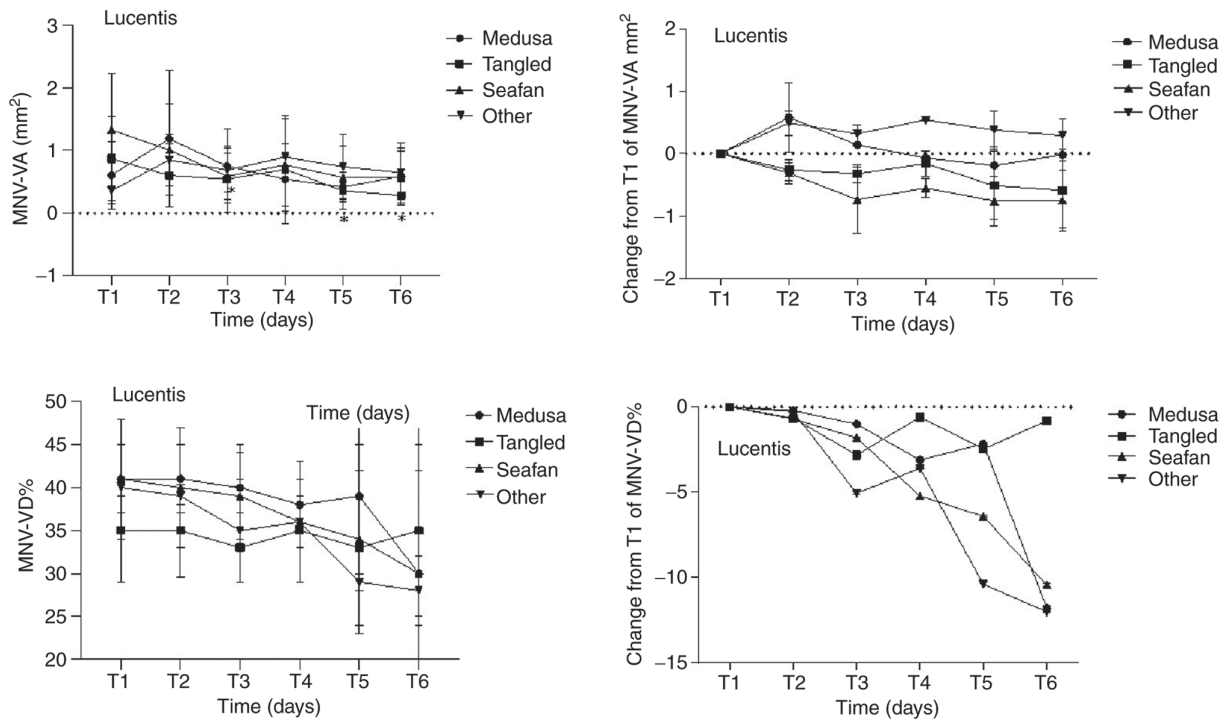


Figure 5. Comparison of MNV parameters before and after treatment for eyes with four distinct MNV patterns of neovascular membrane observed on OCTA. The top row presents mean MNV-VA values (left) and adjusted mean changes in mean MNV-VA (right) from baseline to post-treatment at various time points. The bottom row displays mean MNV-VD ratio values (left) and adjusted mean changes in mean MNV-VD ratio (right) from baseline to post-treatment at different time points. MNV, macular neovascularization; MNV-VA, MNV vascular area MNV-VD, MNV vascular density.

but measurable MNV). Consistent with Tew *et al* (16), there was a higher proportion of eyes with the seafan pattern in the present study (27).

Numerous researchers have examined the structural parameters of MNV, seeking to determine whether variations in these parameters are associated with the prognosis of

Table X. Mean BCVA, CMT and MNV parameters obtained from neovascular age-related macular degeneration patients before and after intravitreal injection.

Group	Mean BCVA (LogMAR)		Mean CMT (μm)		Mean MNV-VA (mm^2)		Mean MNV-VD ratio	
	Baseline	90 days	Baseline	90 days	Baseline	90 days	Baseline	90 days
Conbercept (n=26)	0.97 \pm 0.50	0.78 \pm 0.53	293.71 \pm 145.60	211.94 \pm 51.11	1.34 \pm 1.14	0.79 \pm 0.59	0.40 \pm 0.10	0.34 \pm 0.12
Ranibizumab (n=18)	0.94 \pm 0.54	0.70 \pm 0.47	328.72 \pm 144.80	200.51 \pm 90.29	0.87 \pm 0.71	0.47 \pm 0.35	0.39 \pm 0.06	0.31 \pm 0.11
P-value	0.831	0.639	0.527	0.527	0.166	0.086	0.596	0.573

Data are presented as means \pm standard deviation. $P < 0.05$ was considered to indicate a statistically significant difference. BCVA, best-corrected visual acuity; CMT, central macular thickness; MNV, macular neovascularization; MNV-VA, MNV vascular area; MNV-VD, MNV vascular density.

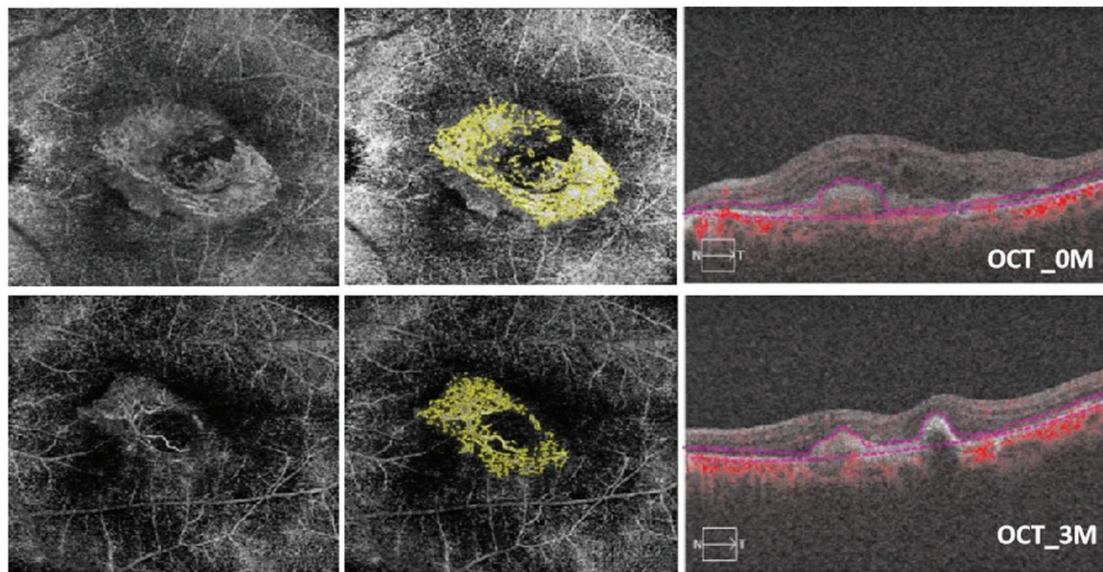


Figure 6. OCTA images of an 83-year-old male patient with seafan pattern MNV who underwent IVR therapy in the right eye. Baseline visual acuity was 1.3 logMAR after three ranibizumab injections in 90 days. In the top left, a 6x6 spectral-domain OCTA image displays the neovascular complex with globular lesions, showing no main vascular entanglement compared with an OCTA *en face* projection image after ranibizumab injection (bottom left). In the top center, the analysis results of ImageJ software correspond to post-treatment (bottom center). The top right OCT image shows the presence of subretinal fluid. In the bottom right, subretinal fluid and subretinal hyper-reflective material were reduced; meanwhile, the BCVA improved to 0.9 logMAR after ranibizumab injection at 3 months (90 days). The MNV-VA decreased from 2.283 mm^2 (baseline) to 1.375 mm^2 (90 days) OCTA, optical coherence tomography angiography; MNV, macular neovascularization; IVR, intravitreal ranibizumab; MAR, minimum resolution angle; MNV-VA, MNV vascular area; BCVA, best-corrected visual acuity.

anti-VEGF treatment (10,28-30). The present study revealed notable improvements in the overall BCVAs across the four MNV pattern groups, coupled with a decrease in structural parameters following anti-VEGF treatment. The two drug treatment cohorts exhibited a statistically significant reduction in CMT, accompanied by a corresponding increase in visual acuity before and after treatment.

This observation aligned with findings from established literature on nAMD, including the CATT study (27,31). Regarding MNV parameters, both the MNV-VA and the MNV-VD ratio showed a decrease after anti-VEGF treatment in the two drug groups. However, these differences did not reach statistical significance. The efficacy of anti-VEGF treatment across diverse MNV patterns has been validated in several studies (16,32,33). The present study observed a significant improvement in visual

acuity among patients with the tangled pattern at five postoperative time points following conbercept injection. Notably, the magnitude of BCVA improvement in this group surpassed that of patients with the other three patterns. The reasons behind the increased efficacy of conbercept in treating complex retinal conditions involving tangled MNV remain somewhat unclear. It was hypothesized that tangled MNV, characterized by vascular masses lacking prominent vessels, might demonstrate heightened sensitivity to conbercept, a fusion protein comprising VEGFR and a recombinant human IgG Fc gene. These findings aligned with the suggestion of Tew *et al* (16) that MNV lacking a main trunk vessel and presenting with improved baseline vision are favorable indicators for visual prognosis. However, the present study differed in that the baseline vision of patients with the tangled pattern was suboptimal.

Furthermore, a significant reduction in both MNV-VA and the MNV-VD ratio was observed among patients with the Medusa pattern after conbercept injection, as compared with those with the other three patterns. Notably, this decrease in MNV parameters did not correspond to a simultaneous increase in visual acuity. Additionally, the improvement in BCVA was minimal in the IVR group throughout the entire experimental observation period. A previous study reported that active MNV on OCTA features a higher incidence of prominent central vessels, dense branching vessels and peripheral arcades in active lesions (34). Thick central main vessels and active lesions often indicate the chronic course of mature neovascularization. Patients with this chronic, mature MNV type are more likely to exhibit an incomplete response to anti-VEGF therapy and may face challenges in achieving significant vision recovery. The results of the present study aligned with the findings of Levine *et al* (35), suggesting that changes in area and density are associated with decreases in the number and diameter of branching vessels.

Notably, the present study demonstrated significant improvements in visual acuity and a decrease in MNV-VA among patients with the seafan pattern in the ranibizumab treatment group. While the change in BCVA improvement was markedly different, the alteration in MNV-VA decrease did not reach statistical significance. Kuehlewein *et al* (25) previously reported that patients with the seafan pattern among type 1 MNV individuals exhibit improved BCVA after ranibizumab therapy. They hypothesize that the small molecular structure of ranibizumab may facilitate its penetration through the RPE layer.

Furthermore, the observations of the present study indicated a decrease in MNV-VA at T3 (7 days after the first injection), followed by some recovery at T4 (30 days after the first injection). This was accompanied by corresponding fluctuations in visual acuity during the same periods. Lumbroso *et al* (36) proposed a 'cycle' of MNV growth, where 24 h post-injection, OCTA shows a reduction in neovascularization with vessels appearing 'broken'. Subsequent 'pruning' of thinner anastomotic stoma and 'loss' of smaller vessels contributed to a reduction in the MNV-VA, making the vascular trunk visible by the 7 to 10th day. As the MNV-VA continued to decrease, re-proliferation of vessels was detected by OCTA at 28-35 days post-injection, with some anastomoses and rings reappearing in areas where vessels had previously 'collapsed'. Told *et al* (37) have also concluded that anti-VEGF drugs can intermittently inhibit angiogenesis, prompting neovascular buds of MNV to undergo a cycle of germination, pruning, and leakage. The findings of the present study aligned with this research.

Among the 44 eyes in the present study, six (13.6%) exhibited other MNV types characterized by an ill-defined shape that could be measured, primarily manifesting irregular 'dendritic', 'filamentous', and 'circular' patterns. The significant decrease in CMT was notable. Long linear vessels are classified as inactive lesions with minimal vascular leakage, demonstrating a favorable response to anti-VEGF drugs as effective anti-leakage agents (26,38-40).

In the present study, no statistical differences were found between the two drug treatment groups in terms of BCVA, CMT and MNV parameters. According to the '3+PRN' regimen of anti-VEGF drugs, the visual gain at 3 months

post-injection can serve as a predictor for long-term visual prognosis (16). Rush *et al* (41) proposed that changes in CNV size on ICGA 2 months after anti-VEGF therapy can aid clinicians in predicting the clinical course of nAMD subjects. An extensive 8-year clinical trial (42), affirming that 3+PRN usage can sustain or enhance the vision of 50% of neovascular AMD patients. Real-world studies further support the efficacy of the 3+PRN regimen, indicating comparable visual benefits to the 3+T&E regimen, albeit with fewer injections, reduced economic burden and increased patient acceptability (43-45). The present study provided quantitative follow-up data for two anti-VEGF drugs over 3 months, administered under the '3+PRN' treatment regimen. It is planned to collect follow-up data for ≥ 12 months to validate our initial conclusions and hypotheses.

The current study presented several limitations that warrant consideration. First, although the study adopted a prospective design, the lack of randomization in the treatment allocation for patients in the two groups, with treatments administered based on patient preferences, introduced a potential source of bias. Second, the cohort of treatment-naïve nAMD patients included in the present study was relatively small and only six eyes exhibited the other pattern of MNV. Additionally, the 3-month follow-up duration was relatively short, resulting in potentially weakened conclusions. The statistical challenge of identifying significant findings amid a vast amount of data might also be a factor in the present study. Undoubtedly, future studies with larger sample sizes and longer follow-up periods are imperative to strengthen the robustness of conclusions drawn. Third, technical limitations, including projection artifacts, segmentation artifacts, and motion artifacts, are inevitable when OCTA collects data on deep neovascularization blood flow. This hinders the ability of the present study to refine and correlate the shape of MNV and the position of MNV (type 1/type 2/mixed MNV).

Acknowledgements

The authors extend their sincere gratitude to Dr Yang Sun (Data Center, Shaanxi Provincial People's Hospital, Xi'an, Shaanxi) for providing invaluable guidance on the statistical methods employed in this manuscript. Dr Sun's expertise significantly contributed to the rigor and accuracy of our analyses.

Funding

The present study received support from the Natural Science Foundation of Shaanxi Province (grant no. 2022JM-517) and the Science and Technology Talents Support Program of Shaanxi Provincial People's Hospital (grant no. 2021JY-37).

Availability of data and materials

The data generated in the present study may be requested from the corresponding author.

Authors' contributions

JL conceived and executed the experiments, analyzed the data and contributed to manuscript editing. ZY conducted the

experiments. XL analyzed the data. DL performed experiments and analyzed data. JY and MD wrote and edited the manuscript. JL and JY confirm the authenticity of all the raw data. All authors read and approved the final manuscript.

Ethics approval and consent to participate

The present study received approval from the Ethics Committee of Shaanxi Provincial People's Hospital [Xi'an, China; approval no. 2022 no.(R002)], in accordance with the Declaration of Helsinki. Written informed consent was obtained from participants as detailed in Materials and methods section of the present study.

Patient consent for publication

Not applicable.

Competing interests

The authors declare that they have no competing interests.

References

- Jonasson F, Fisher DE, Eiriksdottir G, Sigurdsson S, Klein R, Launer LJ, Harris T, Gudnason V and Cotch MF: Five-year incidence, progression, and risk factors for age-related macular degeneration: The age, gene/environment susceptibility study. *Ophthalmology* 121: 1766-1772, 2014.
- Afarid M, Azimi A and Malekzadeh M: Evaluation of serum interferons in patients with age-related macular degeneration. *J Res Med Sci* 24: 24, 2019.
- Apte RS, Chen DS and Ferrara N: VEGF in signaling and disease: Beyond discovery and development. *Cell* 176: 1248-1264, 2019.
- Kim KJ, Li B, Winer J, Armanini M, Gillett N, Phillips HS and Ferrara N: Inhibition of vascular endothelial growth factor-induced angiogenesis suppresses tumour growth in vivo. *Nature* 362: 841-844, 1993.
- Schlottmann PG, Alezzandrini AA, Zas M, Rodriguez FJ, Luna JD and Wu L: New treatment modalities for neovascular age-related macular degeneration. *Asia Pac J Ophthalmol (Phila)* 6: 514-519, 2017.
- Nguyen QD, Das A, Do DV, Dugel PU, Gomes A, Holz FG, Koh A, Pan CK, Sepah YJ, Patel N, *et al.*: Brolicizumab: Evolution through preclinical and clinical studies and the implications for the management of neovascular age-related macular degeneration. *Ophthalmology* 127: 963-976, 2020.
- Borrelli E, Parravano M, Sacconi R, Costanzo E, Querques L, Vella G, Bandello F and Querques G: Guidelines on optical coherence tomography angiography imaging: 2020 Focused update. *Ophthalmol Ther* 9: 697-707, 2020.
- Borrelli E, Sarraf D, Freund KB and Sadda SR: OCT angiography and evaluation of the choroid and choroidal vascular disorders. *Prog Retin Eye Res* 67: 30-55, 2018.
- Jia Y, Bailey ST, Wilson DJ, Tan O, Klein ML, Flaxel CJ, Potsaid B, Liu JJ, Lu CD, Kraus MF, *et al.*: Quantitative optical coherence tomography angiography of choroidal neovascularization in age-related macular degeneration. *Ophthalmology* 121: 1435-1444, 2014.
- Ashraf M, Souka A and Adelman RA: Age-related macular degeneration: Using morphological predictors to modify current treatment protocols. *Acta Ophthalmol* 96: 120-133, 2018.
- Inoue M, Jung JJ, Balaratnasingam C, Dansingani KK, Dhrami-Gavazi E, Suzuki M, de Carlo TE, Shahlaee A, Klufas MA, El Maftouhi A, *et al.*: A comparison between optical coherence tomography angiography and fluorescein angiography for the imaging of type 1 neovascularization. *Invest Ophthalmol Vis Sci* 57: OCT314-OCT323, 2016.
- Hsu CR, Lai TT, Hsieh YT, Ho TC, Yang CM and Yang CH: Combined quantitative and qualitative optical coherence tomography angiography biomarkers for predicting active neovascular age-related macular degeneration. *Sci Rep* 11: 18068, 2021.
- Arrigo A, Aragona E, Bordato A, Amato A, Borghesan F, Bandello F and Parodi MB: Quantitative optical coherence tomography angiography parameter variations after treatment of macular neovascularization secondary to age-related macular degeneration. *Retina* 41: 1463-1469, 2021.
- Shin YI, Kim JM, Lee MW, Jo YJ and Kim JY: Characteristics of the foveal microvasculature in asian patients with dry age-related macular degeneration: An optical coherence tomography angiography study. *Ophthalmologica* 243: 145-153, 2020.
- Su L, Ji YS, Tong N, Sarraf D, He X, Sun X, Xu X and Sadda SR: Quantitative assessment of the retinal microvasculature and choriocapillaris in myopic patients using swept-source optical coherence tomography angiography. *Graefes Arch Clin Exp Ophthalmol* 258: 1173-1180, 2020.
- Tew TB, Lai TT, Hsieh YT, Ho TC, Yang CM and Yang CH: Comparison of different morphologies of choroidal neovascularization evaluated by ocular coherence tomography angiography in age-related macular degeneration. *Clin Exp Ophthalmol* 48: 927-937, 2020.
- Spaide RF, Jaffe GJ, Sarraf D, Freund KB, Sadda SR, Staurengi G, Waheed NK, Chakravarthy U, Rosenfeld PJ, Holz FG, *et al.*: Consensus nomenclature for reporting neovascular age-related macular degeneration data: Consensus on neovascular age-related macular degeneration nomenclature study group. *Ophthalmology* 127: 616-636, 2020.
- Takeuchi J, Kataoka K, Ito Y, Takayama K, Yasuma T, Kaneko H and Terasaki H: Optical coherence tomography angiography to quantify choroidal neovascularization in response to aflibercept. *Ophthalmologica* 240: 90-98, 2018.
- Liang MC, de Carlo TE, Bauman CR, Reichel E, Waheed NK, Duker JS and Witkin AJ: Correlation of spectral domain optical coherence tomography angiography and clinical activity in neovascular age-related macular degeneration. *Retina* 36: 2265-2273, 2016.
- Eandi CM, Ciardella A, Parravano M, Missiroli F, Alovise C, Veronese C, Morara MC, Grossi M, Virgili G and Ricci F: Indocyanine green angiography and optical coherence tomography angiography of choroidal neovascularization in age-related macular degeneration. *Invest Ophthalmol Vis Sci* 58: 3690-3696, 2017.
- Coscas GJ, Lupidi M, Coscas F, Cagini C and Souied EH: Optical coherence tomography angiography versus traditional multimodal imaging in assessing the activity of exudative age-related macular degeneration: A new diagnostic challenge. *Retina* 35: 2219-2228, 2015.
- Roberts PK, Nesper PL, Gill MK and Fawzi AA: Semiautomated quantitative approach to characterize treatment response in neovascular age-related macular degeneration: A real-world study. *Retina* 37: 1492-1498, 2017.
- El Ameen A, Cohen SY, Semoun O, Miere A, Srour M, Quaranta-El Maftouhi M, Oubraham H, Blanco-Garavito R, Querques G and Souied EH: Type 2 neovascularization secondary to age-related macular degeneration imaged by optical coherence tomography angiography. *Retina* 35: 2212-2218, 2015.
- de Carlo TE, Bonini Filho MA, Chin AT, Adhi M, Ferrara D, Bauman CR, Witkin AJ, Reichel E, Duker JS and Waheed NK: Spectral-domain optical coherence tomography angiography of choroidal neovascularization. *Ophthalmology* 122: 1228-1238, 2015.
- Kuehlewein L, Bansal M, Lenis TL, Iafe NA, Sadda SR, Bonini Filho MA, De Carlo TE, Waheed NK, Duker JS and Sarraf D: Optical coherence tomography angiography of type 1 neovascularization in age-related macular degeneration. *Am J Ophthalmol* 160: 739-748.e2, 2015.
- Karacorlu M, Sayman Muslubas I, Arf S, Hocaoglu M and Ersoz MG: Membrane patterns in eyes with choroidal neovascularization on optical coherence tomography angiography. *Eye (Lond)* 33: 1280-1289, 2019.
- Comparison of Age-related Macular Degeneration Treatments Trials (CATT) Research Group; Martin DF, Maguire MG, Fine SL, Ying GS, Jaffe GJ, Grunwald JE, Toth C, Redford M and Ferris FL III: Ranibizumab and bevacizumab for treatment of neovascular age-related macular degeneration: Two-year results. *Ophthalmology* 119: 1388-1398, 2012.
- Told R, Reumueller A, Schranz M, Brugger J, Weigert G, Reiter GS, Sacu S and Schmidt-Erfurth U: OCTA biomarker search in patients with nAMD: Influence of retinal fluid on time-dependent biomarker response. *Curr Eye Res* 48: 600-604, 2023.

29. Faatz H, Rothaus K, Ziegler M, Book M, Spital G, Lange C, Lommatzsch A: The architecture of macular neovascularizations predicts treatment responses to anti-VEGF therapy in neovascular AMD. *Diagnostics (Basel)* 12: 2807, 2022.
30. Arya M, Rashad R, Sorour O, Moulton EM, Fujimoto JG and Waheed NK: Optical coherence tomography angiography (OCTA) flow speed mapping technology for retinal diseases. *Expert Rev Med Devices* 15: 875-882, 2018.
31. Kanadani TCM, Veloso CE and Nehemy MB: Subfoveal choroidal thickness in eyes with neovascular age-related macular degeneration treated with anti-vascular endothelial growth factor agents. *Ophthalmologica* 240: 200-207, 2018.
32. Miere A, Butori P, Cohen SY, Semoun O, Capuano V, Jung C and Souied EH: Vascular remodeling of choroidal neovascularization after anti-vascular endothelial growth factor therapy visualized on optical coherence tomography angiography. *Retina* 39: 548-557, 2019.
33. Miere A, Semoun O, Cohen SY, El Ameen A, Srouf M, Jung C, Oubraham H, Querques G and Souied EH: Optical coherence tomography angiography features of subretinal fibrosis in age-related macular degeneration. *Retina* 35: 2275-2284, 2015.
34. Al-Sheikh M, Iafe NA, Phasukkijwatana N, Sadda SR and Sarraf D: Biomarkers of neovascular activity in age-related macular degeneration using optical coherence tomography angiography. *Retina* 38: 220-230, 2018.
35. Levine ES, Custo Greig E, Mendonça LSM, Gulati S, Despotovic IN, Alibhai AY, Moulton E, Muakkassa N, Quaranta-El Maftouhi M, El Maftouhi A, *et al*: The long-term effects of anti-vascular endothelial growth factor therapy on the optical coherence tomography angiographic appearance of neovascularization in age-related macular degeneration. *Int J Retina Vitreous* 6: 39, 2020.
36. Lumbroso B, Rispoli M and Savastano MC: Longitudinal optical coherence tomography-angiography study of type 2 naive choroidal neovascularization early response after treatment. *Retina* 35: 2242-2251, 2015.
37. Told R, Reiter GS, Schranz M, Reumueller A, Hacker V, Mittermueller TJ, Roberts PK, Sacu S and Schmidt-Erfurth U: Correlation of retinal thickness and swept-source optical coherence tomography angiography derived vascular changes in patients with neovascular age-related macular degeneration. *Curr Eye Res* 46: 1002-1009, 2021.
38. Arrigo A, Aragona E, Bordato A, Amato A, Borghesan F, Bandello F and Battaglia Parodi M: Morphological and functional relationship between OCTA and FA/ICGA quantitative features in AMD-related macular neovascularization. *Front Med (Lausanne)* 8: 758668, 2021.
39. Ahmed M, Syrine BM, Nadia BA, Anis M, Karim Z, Mohamed G, Hachemi M, Fethi K and Leila K: Optical coherence tomography angiography features of macular neovascularization in wet age-related macular degeneration: A cross-sectional study. *Ann Med Surg (Lond)* 70: 102826, 2021.
40. Carnevali A, Cicinelli MV, Capuano V, Corvi F, Mazzaferro A, Querques L, Scorcia V, Souied EH, Bandello F and Querques G: Optical coherence tomography angiography: A useful tool for diagnosis of treatment-naïve quiescent choroidal neovascularization. *Am J Ophthalmol* 169: 189-198, 2016.
41. Rush RB, Rush SW, Aragon AV II and Ysasaga JE: Evaluation of choroidal neovascularization with indocyanine green angiography in neovascular age-related macular degeneration subjects undergoing intravitreal bevacizumab therapy. *Am J Ophthalmol* 158: 337-344, 2014.
42. Horner F, Lip PL, Clark H, Chavan R, Sarmad A and Mushtaq B: Real-world visual and clinical outcomes for patients with neovascular age-related macular degeneration treated with intravitreal ranibizumab: An 8-year observational cohort (AMD8). *Clin Ophthalmol* 13: 2461-2467, 2019.
43. Jacob J, Brié H, Leys A, Levecq L, Mergaerts F, Denhaerynck K, Vancayzele S, Van Craeyveld E, Abraham I and MacDonald K: Six-year outcomes in neovascular age-related macular degeneration with ranibizumab. *Int J Ophthalmol* 10: 81-90, 2017.
44. Gillies MC, Campain A, Barthelmes D, Simpson JM, Arnold JJ, Guymer RH, McAllister IL, Essex RW, Morlet N and Hunyor AP; Fight Retinal Blindness Study Group: Long-term outcomes of treatment of neovascular age-related macular degeneration: Data from an observational study. *Ophthalmology* 122: 1837-1845, 2015.
45. Rofagha S, Bhisitkul RB, Boyer DS, Sadda SR and Zhang K; SEVEN-UP Study Group: Seven-year outcomes in ranibizumab-treated patients in ANCHOR, MARINA, and HORIZON: A multicenter cohort study (SEVEN-UP). *Ophthalmology* 120: 2292-2299, 2013.



Copyright © 2024 Li et al. This work is licensed under a Creative Commons Attribution-NonCommercial-NoDerivatives 4.0 International (CC BY-NC-ND 4.0) License.